Criteria-Based Modulation for Multilevel Inverters

Kfir J. Dagan and Raul Rabinovici

***Abstract*—Pulse width modulation schemes are aimed at adjusting the fundamental component while reducing the harmonic content of an inverter output voltage or current. This paper addresses the topic of optimal inverter operation in reference to a given objective function. The objective function could embody either a single performance criterion, such as voltage or current total harmonic distortion (THD), or a weighted sum of multiple criteria. The proposed method ensures primacy of the chosen solution while imposing no restriction over its modulation index. In particular, operating the inverter by the chosen solution would result in performances superior to any other modulation scheme commutating in an equal number of switching angles per fundamental cycle. The proposed method allows for the consideration of practical inverter constraints and prevents the possibility of impractical switching sequence. A detailed investigation of the method is given, accompanied by two practical cases minimizing, respectively, phase-voltage THD and line-current THD of a three-level inverter. Selected simulation and experimental results are presented to validate the theoretical part.**

***Index Terms*—Direct search, harmonics, optimal, pulse width modulation (PWM), total harmonic distortion (THD), voltage-source inverter (VSI).**

I. Introduction

MODULATION techniques for multilevel inverters have been the subject of intensive research in the last few decades. A wide variety of methods, different in concept and performances [1], [2], have been developed and analyzed in the literature. Amongst the various methods available, the most frequently used are sinusoidal pulse width modulation (SPWM), space vector (SV), and selective harmonic elimination (SHE) [3]–[5].

Given an inverter application, the various modulation schemes are generally determined by performance criteria with total harmonic distortion (THD) being the most frequently used [6]. Other common criteria would be specific harmonic-amplitude restriction set by recommendation and standards such as IEEE Std. 519 [7], peak common-mode voltage (CMV) [8], rms CMV [9], and harmonic distortion factor (HDF) [10].

Numerous papers have contributed to the topic of PWM performance analysis. In [11], performance criteria were developed to allow comparison of various optimal-PWM strategies in means of harmonic losses, pulsating torque, and peak current. Another comparison of PWM switching schemes in terms of various performance criteria is given in [2].

Manuscript received February 14, 2014; revised May 11, 2014 and July 25, 2014; accepted August 22, 2014. Date of publication October 8, 2014; date of current version April 15, 2015. Recommended for publication by Associate Editor J. R. Rodriguez.

The authors are with the Department of Electrical and Computer Engineering, Ben-Gurion University of the Negev, Beer-Sheva 84105, Israel (e-mail: kdagan@gmail.com; rr@ee.bgu.ac.il).

Color versions of one or more of the figures in this paper are available online at http://ieeexplore.ieee.org.

Digital Object Identifier 10.1109/TPEL.2014.2362171

Inverter THD performance is another topical issue in the literature. Harmonic analysis of various PWM methods, based on double Fourier series, was presented in [2] and established in [12]. A further spectral analysis of carrier-based PWM is presented in [13]. This paper uses 1-D Fourier series to formulate closed-form expressions for the individual harmonics. In [14], phase-voltage THD of a staircase waveform is formulated based on the waveform switching angles. A more generic formula, evaluating THD of a general multilevel phase voltage is given in [15]. Another extension of [14] is given in [6], where the line-voltage THD of a staircase waveform is formulated and compared to various approximation methods. Utilization of genetic algorithm optimization to minimize the line-voltage THD of a staircase waveform is presented in [16]. The minimization is obtained via direct evaluation of the line-voltage waveform and its resulting THD index. Another work concerning reduced THD PWM waveform is provided in [17]. This paper employs variable sampling frequency PWM to reduce line-current THD. Finally, comparison of symmetrical and nonsymmetrical selective harmonic elimination PWM techniques in terms of THD is presented in [10]. The two schemes are also compared in light of the number of harmonics eliminated, harmonic spectrum profile, and HDF.

Reduced CMV PWM methods also draw increasing attention in the literature. This interest is due to various problems associated with CMV in electrical systems. These problems include, amongst others, electromagnetic interference [18], motor insulation stress, and bearing current which may ultimately result in premature motor bearing failure [19]. In [20], interleaved carriers were employed to enhance the CMV performances of ordinary sine PWM. This paper presents improvement of both peak and rms levels of the output CMV. In [21], the contribution of zero SVs to the CMV level in space vector modulation (SVM) was acknowledged and demonstrated. As a natural continuation of [21], reduced CMV modulation schemes have emerged [8], [22]–[25]. While slightly different in performances, they all share limited modulation index range or obtain high CMV spikes when inverter dead time is introduced. Tallam *et al.* [26] proposed a modified reduced CMV modulation scheme, which is impervious to inverter dead time effect and offers extended modulation index range. Another approach for dealing with inverter dead time appears in [27]. In this paper, an optimal CMV reduction PWM technique invariant under dead time, is recommended. The CMV is shown to be reduced to one-third in a diode front end inverter. An equivalent modified SVM methods for current-source inverters (CSI) also appear in the literature. Such strategy is given by [28], where a nonzero state modulation techniques are adapted to reduce CMV levels in an SVM CSI.

Another reduced CMV strategy is proposed in [29]. The proposed method utilizes a smoothed transition between two SHE schemes. In this paper, M-SHEPWM scheme is used to control

the inverter at frequencies smaller than 0.9 of the motor rated frequency. The scheme employs elimination of low-order triplen harmonics to achieve reduced CMV levels. For higher frequencies ($\geq$0.9 motor rated frequency), a C-SHEPWM scheme is employed, which eliminates only nontriplen harmonics. As a result the proposed method generates high CMV levels when operating close to the inverter nominal frequency.

Another optimal PWM method for low switching frequency is reported in [30]. In this paper, a gradient method is used to solve a constraint optimization problem of a normalized THD objective function. The proposed scheme is investigated in light of a three- and five-level inverter topologies.

While large number of optimal modulation strategies appears in the literature, there is no integral comparison available. The lack of comprehensive comparison tool makes the process of choosing the optimal modulation scheme an impossible mission. In addition, optimization-based methods could fall into a local rather than a global extremum of their objective function.

This paper extends the study presented in [31], where the criteria-based modulation (CBM) method was introduce. This paper facilitates a performance-based method to determine the optimal sequence for a given inverter application. The proposed method features low switching frequency, which reduces the switching losses of power switching devices [30]. Lower switching frequency is particularly preferable in medium-voltage drives, owing to the higher switching losses of their semiconductor devices [32]. The supplementary contribution of this paper with reference to [31] is as follows. It thoroughly describes the CBM method and its application to three-phase medium-voltage inverters. Specifically, this paper presents discusses the general case of minimizing the weighted THD (WTHD) [33] of an inverter output waveform. The latter is of great importance as it reflects on the current THD of an inverter output waveform for the general load case. This paper presents experimental results obtained using a three-level three-phase voltage-source inverter (VSI). In addition, this paper presents the dynamic response of the system to a step change in the fundamental amplitude. Finally, this paper provides a complexity analysis of the proposed algorithm alongside an evaluation of the solution set size as a function of system parameters.

Given a criteria-based objective function, a direct search is initiated to find the optimal switching sequence. The obtained solution ensures optimal inverter performance in terms of the defined criterion and does not fall into local extremum. In particular, operating according to the chosen switching sequence ensures performances superior to any other modulation scheme with an equal number of commutations. The proposed method could easily take into account application constraints such as inverter dead time. The proposed method may be used by inverter drive engineers to determine the optimal commutation strategy for a given motor drive application.

The remainder of this paper is as follows. In Section II, the CBM algorithm is fully described. In Section III, practical cases are solved and discussed in terms of optimal inverter performances. The performances of the selected solutions are then validated and analyzed using MATLAB simulations. Following, selected experiment results are presented in Section IV to back up theoretical and simulation sections. Finally, conclusions are presented and discussed in details in Section V.

TABLE I
BLANK CBM LOOK-UP TABLE

#	m_a	α_1	α_2	$\cdots$	α_N	$\mathcal{W}$
1	$m_{a\,1}$			$\cdots$		
1	$m_{a\,2}$			$\cdots$		
$\vdots$	$\vdots$	$\vdots$	$\vdots$	$\ddots$	$\vdots$	$\vdots$
L	$m_{a\,L}$			$\cdots$		

$\#$, m_a, $\mathcal{W}$, and α_i are column headings denoting, respectively, table row number, modulation index, objective function, and the ith switching angle; $i = 1, 2, \ldots, N$. $m_{a\,j}$ denotes the modulation index level of the jth row; $j = 1, 2, .., L$.

II. CBM

The CBM addresses the topic of optimal inverter operation. Given a criteria-based objection function, a direct search is initiated to find the optimal commutation sequence for a given inverter. The search is performed offline, for each modulation index, while at its end, a look-up table (LUT) is constructed. The LUT could be utilized by online PWM controllers [34]–[37] to maintain optimal inverter performances.

The rest of this section describes the CBM process.

A. Initialization

Given a criteria set $\mathcal{C} = \{\mathcal{C}_1, \mathcal{C}_2, \ldots, \mathcal{C}_M\}$ and the corresponding weights $\{W_1, W_2, \ldots, W_M\}$, we define the objective function $\mathcal{W}$ to be

$$\mathcal{W}(\mathcal{C}_1, \mathcal{C}_2, \ldots, \mathcal{C}_M, W_1, W_2, \ldots, W_M) = \frac{\sum_{i=1}^{M} W_i \mathcal{C}_i}{\sum_{i=1}^{M} W_i}. \quad (1)$$

For a single criterion, there would be only one criteria member set $\mathcal{C}_1$ and a single weight $W_1 = 1$. The resulting objective function would then be $\mathcal{W} = W_1 \cdot \mathcal{C}_1 = \mathcal{C}_1$. Practical examples for this case are provided in Sections III and IV. A more general case would involves two criteria and two weights. This could be the case when attempting to minimize both phase- and line-voltage THDs. In this case, $\mathcal{C}_1 = \mathrm{THD}_{V_{\mathrm{Ph}}}$ and $\mathcal{C}_2 = \mathrm{THD}_{V_{\mathrm{Line}}}$. The corresponding weight could then be W_1 and $W_2 = 1 - W_1$. The resulting objective function would, therefore, be

$$\mathcal{W}(\mathcal{C}_1, \mathcal{C}_2, W_1, W_2) = W_1 \mathcal{C}_1 + (1 - W_1)\mathcal{C}_2. \quad (2)$$

The aforementioned is useful when both line-voltage THD and the rms value of the CMV is important. This notion is discussed in Section III-A.

Next we construct a blank LUT. This table will be used in the CBM algorithm phase to log all optimal commutation sequences based on the objective function $\mathcal{W}$. Table I depicts an example $L \times (N + 2)$ blank LUT (excluding headings). As can be seen, table size is determined by the number of commutations per fundamental cycle N and the number of modulation index levels L. The number of commutations N is generally a tradeoff between line current THD and switching power losses

[38], [39]. L is determined with accordance to the desired modulation index range and resolution.

Higher modulation index resolution and/or range would result in larger number of modulation index levels $m_{a1}, m_{a2}, \ldots, m_{aL}$.

Based on application constraints, the set of all valid switching sequences is constructed

$$\mathcal{S} = \{S_1, S_2, \ldots, S_K\} \tag{3}$$

where $S_i,\ i = 1, \ldots K$, is a single sequence with N consecutive switching angles. An example of inverter constraint would be transistor minimum turn ON and OFF times. This constraint is met by

$$\min\{\alpha_1/2, \alpha_2 - \alpha_1, \alpha_3 - \alpha_2, \ldots, \alpha_N - \alpha_{N-1} \times \pi/2 - \alpha_N/2\} < t_{\min} \tag{4}$$

where $\alpha_{\min}$ is the transistor's minimum turn on t_{don} or turn off t_{doff} in radians. The condition expressed in (4) could be easily applied using a set of nested FOR loops. An example MATLAB code and a complexity analysis is given in Appendix B.

B. CBM Algorithm

This section describes the CBM algorithm assuming the initialization phase discussed in the previous section was carried out.

The CBM process evaluates the objective function $\mathcal{W}$ for each valid sequences in $\mathcal{S}$. In each iteration, the objective function mark of the current sequence $\mathcal{W}_i$ is obtained and compared with the value listed in the corresponding row of Table I. Whenever $\mathcal{W}_i$ is superior to the value listed in the table, the switching angles and objective function mark of the current sequence are assigned to the corresponding table row. At the end of this process, a complete CBM table listing the optimal sequences for each modulation index level is obtained. Following is a description of the CBM algorithm:

1) set $i = 1$;
2) select the ith commutation sequence S_i;
3) evaluate objective function mark $\mathcal{W}_i$ associated with S_i;
4) evaluate modulation index m_a^i associated with S_i;
5) locate the table row whose modulation index entry corresponds to m_a^i;
6) IF the corresponding objective function mark is EITHER blank OR inferior than $\mathcal{W}_i$:
   a) replace it with $\mathcal{W}_i$;
   b) replace corresponding sequence with S_i.
7) set $i = i + 1$;
8) IF $i \leq K$ JUMP to step 2;
9) delete $\mathcal{W}$ and # columns;
10) terminate algorithm.

Step 5 would assign the current modulation index mark m_a^i to the table row whose modulation index is the closest to m_a^i. Alternatively, S_i is assigned to a table row n if the following expression holds

$$|m_a^i - m_{an}| = \min_{j \in (1,L)} |m_a^i - m_{aj}|. \tag{5}$$

TABLE II
COMPLETE CBM LOOK-UP TABLE

m_a	α_1	α_2	$\cdots$	α_N
m_{a1}	α_{11}	α_{12}	$\cdots$	α_{1N}
m_{a2}	α_{21}	α_{22}	$\cdots$	α_{2N}
$\vdots$	$\vdots$	$\vdots$	$\ddots$	$\vdots$
m_{aL}	α_{L1}	α_{L2}	$\cdots$	α_{LN}

α_{ij} denote the jth switching angle corresponding to the ith modulation index level $m_{ai}, i = 1, 2, .., N,\ j = 1, 2, .., L$.

This allows for a modulation index margin, $\widetilde{m_a}$, equals to half of the difference between modulation index levels of two consecutive rows, i.e., $\widetilde{m_a} = (m_{aj} - m_{a(j+1)})/2$. $\widetilde{m_a}$ is a function of the initialization parameter L. The modulation index margin $\widetilde{m_a}$ reflects on the size of each subset, and thus, on the diversity of the objective function values within each subset as will be expressed in Sections III and IV.

Employing a direct-search approach is beneficial, where there exists discontinuities of the switching angles with reference to m_a. As the CBM algorithm goes through every valid solution set, it would always obtain the absolute extremum of $\mathcal{W}$ as long as $\mathcal{S}$ contains all valid solutions. This is not the case with general optimization algorithms where discontinuity of the switching angles could lead to converging to local minima, or even divergence of the algorithm [40]. Another characteristic of the direct search nature of the CBM is its independence on the algorithm starting point. This is an advantage over conventional PWM optimization methods that are highly insensitive to the initial conditions.

The aforementioned algorithm is performed offline to provide the complete CBM LUT shown in Table II. It should be noted that table headings row and modulation index column are not needed for the operation of the online controller. Hence, in practice, an array of size $L \times N$ is uploaded to the online controller

Operating the inverter according to Table II would ensure inverter performances superior, or equal, to those of any other modulation strategy operating at an equal number of switching angles.

Fig. 1(a) depicts the CBM sequence set $\mathcal{S}$ in a 3-D space. Each black dot corresponds to a specific sequence in $\mathcal{S}$ through a background matrix. The simplified representation in Fig. 1(a) enables an easy comparison of several switching sequences with reference to the three ordinates: phase-voltage THD, line-current THD, and fundamental amplitude of the output waveform.

The above representation also provides graphical notion to the CBM process. Consider the 2-D subset obtained by intersecting the gray translucent plane with $\mathcal{S}$ at a fundamental amplitude 1125 V. This 2-D CBM map—shown in Fig. 1(b)—contains all members in $\mathcal{S}$ with fundamental amplitude 1125 V. Comparing the subset members according to a single ordinate, s.a. the phase-voltage THD, corresponds to the single criterion case of $\mathcal{C}_1 = \mathrm{THD}_{V_{\mathrm{Ph}}}$ and weight W_1 described in Section II-A. The process of attributing each sequence to a relevant LUT row (step 5 of the algorithm) is similar to the above intersection

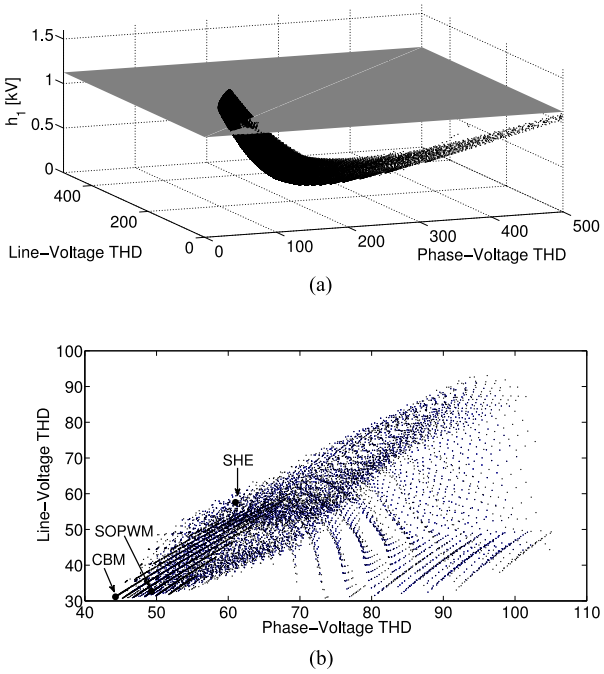

Fig. 1. CBM sequences set S. (a) All valid switching sequences. (b) Valid sequences corresponding to modulation index $m_a = 0.9$ and $\widetilde{m_a} = 0.05$.

with an addition predefined margin expressed by the modulation index margin $\widetilde{m_a}$ in Section II-A. The resulting optimal CBM sequence and the corresponding SHE, and Synchronous Optimal PWM (SOPWM) [30] sequences used as a reference in this paper are depicted by black bullets. In the general case of M criteria and weights, an M-dimensional Euclidean space would be constructed.

All sequences considered in this paper maintain odd-function quarter wave symmetry with three switching angles per quarter wave cycle. Nonetheless, by eliminating the dependence on the switching characteristic, i.e., by ignoring the exact values of the switching angles in the CBM map, general symmetry sequences could be considered. This scheme could be also used to compare between sequences with different number of switching angles and/or different number of voltage levels.

III. Simulation Results

This section presents selected simulation results illustrating the aforementioned CBM method. The simulation parameters are summarized in Table III. All CBM solutions presented in this paper were obtained using MATLAB/Simulink and compared to their corresponding conventional SHE and SOPWM methods. Harmonic components up to the order of 97 were considered.

The conventional SHE solution was obtained by minimizing the Euclidean norm of an amplitude error vector $\vec{A}$ using MATLAB's `fmincon.m`. In general, three switching angles per quarter wave cycle enable the adjusting of the fundamental component amplitude and eliminating two additional harmonics. The resulting amplitude error vector is, therefore

$$\|\vec{A}\| = \sqrt{(h_1 - \hat{h}_1)^2 + h_m^2 + h_n^2} \tag{6}$$

TABLE III
Simulation Parameters Summary

Type	Value	Comments
	RLE Load	
R	0.86 Ω	per-phase
L	23 mH	per-phase
E	$h_1 - (R + j\omega L) \cdot I\text{ph}$	phase A
	General simulation parameters	
f	50 Hz	Fundamental frequency
N	3	Number of switching angles
m_a	0.9/0.5	Modulation index
V_{DC}	350 V	DC-bus voltage
t_{min}	10 uS	Min. turn-on and turn-off
PC	DELL XPS13	Laptop/simulation host

where $\hat{h}_1$, h_1, h_m, and h_n denote, respectively, desired fundamental component amplitude, amplitude of the actual fundamental component, and amplitude of the mth and nth harmonics.

In Section III-A, a phase-voltage THD minimization is discussed. In this section, the SHE solution was obtained by adjusting the fundamental amplitude according to the desired modulation index and eliminating the third and fifth harmonics, i.e., $m = 3$ and $n = 5$ in (6). In Section III-B, the process of minimizing the WTHD is discussed. As in this case, triplen harmonics are not taken into account, the SHE solution was obtained by adjusting the fundamental component accordingly and eliminating the fifth and seventh harmonics, i.e., $m = 5$ and $n = 7$ in (6).

The SOPW solution was obtained similarly to the process described in [30]. The number of angles per quarter wave cycle N was set to 3. The objective function was set to phase-voltage THD in Section III-A and WTHD in Section B. Following, the initial switching sequence was derived as follows. First, switching angles α_2 and α_3 where drawn using MATLAB function `randn.m`. These angles where then used to calculated the exact value of switching angle α_1 using (11) of [30]. Following, the objective function mark corresponding to the obtained sequence was evaluated. The aforementioned process was repeated 200 times. At the end of this process, the optimal objective function mark and its corresponding switching sequence were logged.

The optimization process described in [30] was performed using MATLAB function `fmincon.m`. The initial sequence obtained in the initialization process, the tolerance level, the linear constraint over the switching angles, and the nonlinear constraint formulated by (11) of [30], where passed as function parameters.

A. Phase-Voltage THD

Phase-voltage THD, expressed in (7), is a commonly used quality index in inverter drives [30], [41]. When paired with line-voltage THD, it can be used to evaluate the rms values of the CMV. This section provides simulation results and analysis of the CBM method with a phase-voltage THD objective function

$$\mathcal{W} = \text{THD}_{V_{\text{Ph}}} = 100\frac{\sqrt{\sum_{i=2}^{\infty} h_i^2}}{h_1}. \tag{7}$$

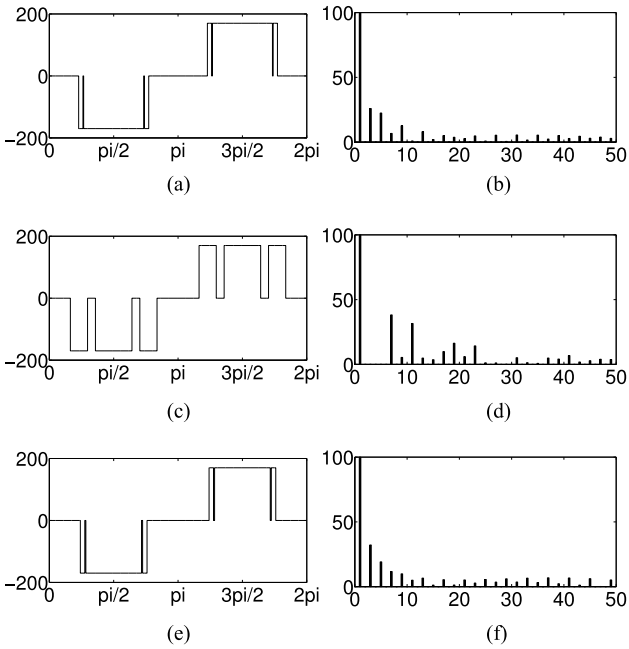

Fig. 2. Phase-voltage angle [rad] and normalized frequency domain representations corresponding to $m_a = 0.9$; Minimum WTHD CBM (a)–(b), SHE (c)–(d), and SOPWM (e)–(f). CBM, SHE, and SOPWM switching angles corresponding to quarter fundamental cycle are, respectively, (0.7156, 0.8203, 0.8378), (0.5132, 0.9329, 1.1250), and (0.7568, 0.8651, 0.8913) in radians.

TABLE IV
SIMULATION INDICES SUMMARY

Index	CBM	SHE [47]	SOPWM [30]
Phase-Voltage THD	42.3%	58.8%	47.0%
Line-Voltage THD	29.1%	57.1%	30.3%
Phase-Voltage THD	98.4%	105.4%	112.0%
Line-Voltage THD	60.5%	81.6%	71.6%
WTHD	4.4%	5.7%	7.0%

Minimum phase-voltage (gray) and WTHD sequences corresponding to, respectively, $m_a = 0.9$ and $m_a = 0.5$.

In terms of the CBM process described in Section II, a single criterion $\mathcal{C}_1 = \mathrm{THD}_{V_{\mathrm{Ph}}}$ is used alongside a single weight $W_1 = 1$. The resulting objective function is therefore $\mathcal{W} = W_1 \cdot \mathcal{C}_1 = \mathrm{THD}_{V_{\mathrm{Ph}}}$.

Fig. 2 shows simulation results for minimum phase-voltage THD CBM, SHE and SOPWM solutions corresponding to $m_a = 0.9$ and $\widetilde{m_a} = 0.05$. The SHE solution was adjusted to maintain the desired fundamental amplitude while eliminating the third and fifth harmonics. Both CBM and SOPWM solutions were obtained using (7).

Angle and normalized frequency domains representation of the CBM solution are shown, respectively, in Fig. 2(a) and (b). The corresponding representations of the SHE solution are shown, respectively, in Fig. 2(c) and (d). Representations of the SOPWM solution are shown, respectively, in Fig. 2(e) and (f). Phase- and line-voltage marks of the three solutions are summarized in Table IV.

Close examination of Fig. 1(b) reveals that there exist numerous switching sequences superior to the SHE solution in both phase- and line-voltage THD marks. This is due to the fact that eliminating the low-order harmonics does not necessarily result in optimal phase- or line-voltage THDs. It should be noted that the SHE method does not guarantee uniqueness of its solutions [42], [43]. The SHE solution is highly dependent on the initial switching sequence as well as on the optimization method used. As a result, there might exist a SHE solution providing better phase- and/or line-voltage THD levels than those presented in Table IV. Nonetheless, there exist no SHE solution with phase-voltage THD lower than the one obtained using the CBM method. This can be deduced from Fig. 2(b), which indicates that the solution providing the lowest phase-voltage THD does not contain zero value for neither the odd harmonics.

Comparing the marks obtained for the minimum phase-voltage THD CBM and SOPWM solutions shows superiority of the CBM solution. The phase-voltage THD obtained using the SOPWM is 10.4% higher than the one obtained using the CBM solution. The advantage of the CBM solution could be due to its direct search approach. As a direct search algorithm, the CBM does not fall into local minima but rather converges to the optimal solution. Superiority of the CBM mark could be also attributed to the modulation index margin $\widetilde{m_a}$. As mentioned earlier, $\widetilde{m_a}$ extends the solution set by admitting solutions with modulation indices slightly different than 0.9, and thus, diverse the possible THD marks. This is not possible with the SOPWM methods, which requires an tight objective function tolerance [30].

Comparison of the CBM and SOPWM marks for line-voltage THD also favors the CBM method. The line-voltage THD obtained using the CBM scheme shows a modest 3.2% improvement in comparison to its counterpart. The difference between the two solutions also indicates increased triplen harmonic content of the SOPWM solution. This triplen harmonic content would be expressed in increased CMV rms values, which adversely affects the reliability of the motor, as well as the electromagnetic compatibility of the motor drive and protection devices [44]. The relation between phase-voltage THD, line-voltage THD, and rms values of the CMV is expressed by

$$\mathrm{THD}^2_{V_{\mathrm{Ph}}} = \mathrm{THD}^2_{V_{\mathrm{Line}}} + \mathrm{CMV}^2_{\mathrm{rms}}. \tag{8}$$

A detailed formulation of (8) is presented in Appendix A.

Another advantage of the CBM over the SOPWM method would be the lack of modulation index restriction. The CBM could be applied with any given modulation index value and is not confined to a certain interval such as in the SOPWM case [30].

B. WTHD

Minimizing line-current THD is another approach for optimal inverter operation. Line-current THD depends on motor parameters and operating conditions [45]. In the absence of an accurate motor model, WTHD [13], [33] can be used to evaluate line-current quality. WTHD, also known as harmonic current

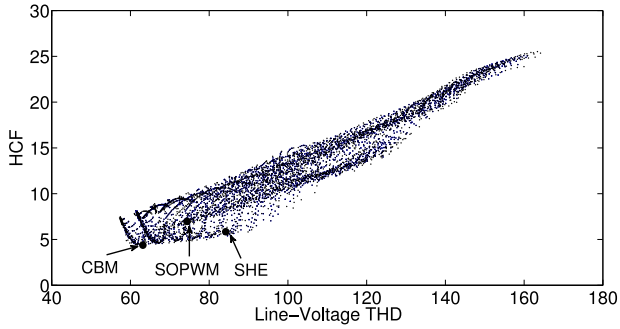

Fig. 3. Valid switching sequences corresponding to modulation index $m_a = 0.5$ and $\widetilde{m_a} = 0.05$.

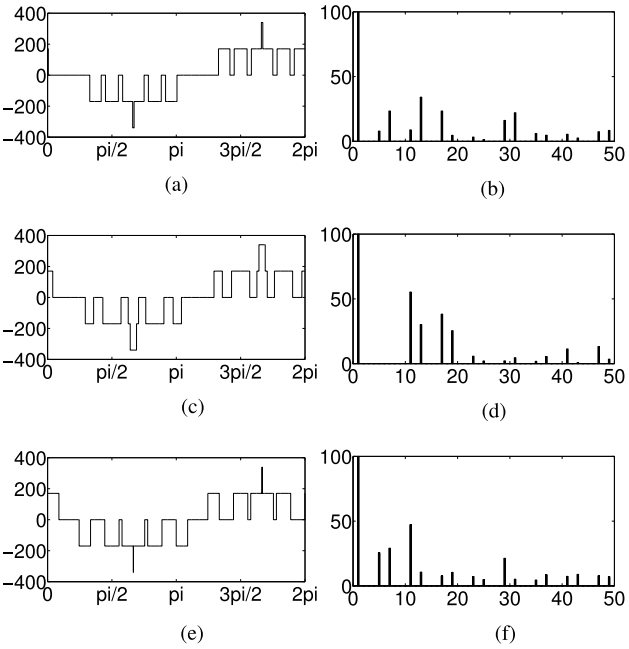

Fig. 4. Line-voltage angle [rad] and normalized frequency domain representations corresponding to $m_a = 0.5$; Minimum WTHD CBM (a)–(b), SHE (c)–(d), and SOPWM (e)–(f). CBM, SHE, and SOPWM switching angles corresponding to quarter fundamental cycle are, respectively, (1.0297, 1.3090, 1.4137), (0.9210, 1.1239, 1.3491), and (0.7703, 1.0490, 1.3965) in radians.

gactor (HCF) [46], is expressed as follows:

$$\text{WTHD} = 100\frac{\sqrt{\sum_{\substack{k=1\\ i=6k\pm1}}^{\infty}\left(\frac{h_i}{i}\right)^2}}{h_1}. \tag{9}$$

The tight correlation between line-current THD and WTHD will be further discussed in Section IV.

Fig. 3 shows a 2-D subset of $\mathcal{S}$ with reference to line-voltage THD and WTHD indices. This subset contains all valid switching sequences corresponding to m_a=0.5 and $\widetilde{m_a}$=0.05. As with the previous case, CBM, SHE, and SOPWM sequences are shown. Notable point is the approximately linear relationship between WTHD and line-voltage THD indices as apparent in the figure.

Fig. 4 illustrates the three solutions in angle [rad] and frequency domain representations. The SHE solution was aimed at properly adjusting the fundamental amplitude while eliminating the fifth and seventh harmonics. Both CBM and SOPWM solution were obtained by utilizing (9).

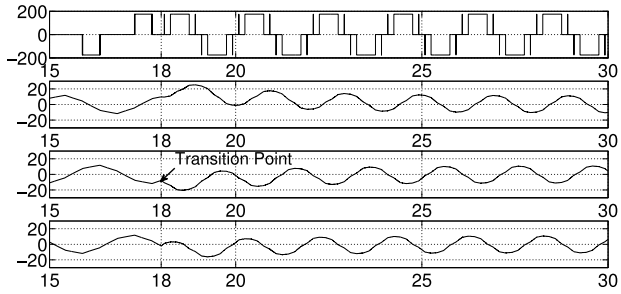

Fig. 5. Dynamic response to a step function; from top to bottom: phase voltage and line currents for a, b, and c phase; time [ms].

The sequences' phase-voltage THD, line-voltage THD, and WTHD are summarized in Table IV. As with the minimum THD case, utilization of the CBM method with objective function (9) provides superior marks for all indices. The distinct advantage of the CBM over SHE and SOPWM methods could be attributed to both its direct search approach and modulation index margin $\widetilde{m_a}$. It should be noted that the relatively high phase-voltage THD marks obtained for all three waveforms are due to the considerably low modulation index m_a.

C. Dynamic Response to Step Change in the Inverter Fundamental Amplitude

Fig. 5 shows simulation results for a V/f step change transition from an initial operating point $V_{\text{init}}/f_{\text{init}} = 113.75\,\text{V}/35\,\text{Hz}$ to a consequent operating point $V_{\text{fin}}/f_{\text{fin}} = 157.5/50\,\text{Hz}$. Sequences were obtained by minimizing phase-voltage THD using a CBM algorithm. The sequence following the transition is the exact CBM sequence obtained in Section III-A.

As can be seen, the system response to a step change is relatively smooth due to the high inertia of the load. In addition, the convergence time is very short, lasting no more than three fundamental cycles. The aforementioned is attributed to the large time constants of high-power rotating machines. As a result, the controller bandwidth is of somewhat reduced importance in comparison to lower power applications.

IV. Experimental Results

This section presents selected experimental results to back up the theoretical and simulation sections. All waveforms presented in this section were captured using a TDS210 Tektronix Digital Real-Time Oscilloscope and exported to MATLAB environment for spectral analysis and figure generation. The performances of the proposed algorithm have been experimentally investigated through a three-phase three-level IGBT-based neutral-point clamped inverter system. System setup diagram and picture are shown, respectively, in Fig. 6(a) and (b). Experiments were carried out for numerous motor operating conditions. Selected results are presented below. Table V summarized

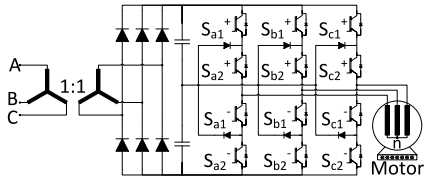

(a)

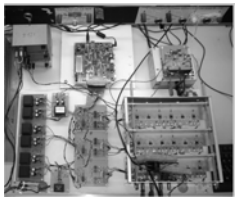

(b)

Fig. 6. (a) Circuit diagram and (b) laboratory setup.

TABLE V
SYSTEM PARAMETERS SUMMARY

Type	Value	Comments
	Motor	
Family	KS100L	YONA USPIZ
P/N	AS 218/06	Y configuration
Power	0.75 kW	
Velocity	2870	
Voltage	400/230	Y/Δ
Current	6.1/10.6	Y/Δ
Frequency	50 Hz	
	Inverter	
IGBT	IRG4BC20FD	
$t_{\min}$	10 uS	Min. switching times
DC Capacitors	$3 \times 470 = 1410$ uF/450 V	Per clamping capacitor Electrolytic JAMICON
FPGA	Artix-7 XC7A100T	Xilinx

the various system parameters. Similar to Section III, harmonic components up to the order of 97 were considered.

A. Phase-Voltage THD

Fig. 7 shows experimental results for the minimum phase-voltage THD CBM and SHE waveforms. The time- and frequency-domain waveforms correspond to $m_a = 0.9$ and $\widetilde{m_a} = 0.09$. The waveforms switching sequences are similar to the ones obtained in Section III-A. Table VI summarizes the indices marks for the CBM and SHE waveforms. Both CBM and SHE marks are similar to those obtained via simulations. Unlike the SHE solution, the third and fifth harmonics of the CBM sequence are nonzero. Nonetheless, the CBM waveform shows superior marks for both phase- and line-voltage THDs. These results are consistent with those of Section III-A.

B. WTHD

Fig. 8 shows time- and frequency-domain representations of the minimum WTHD CBM, SHE, and SOPWM waveforms for $m_a = 0.5$ and $\widetilde{m_a} = 0.05$. The waveforms' indices marks

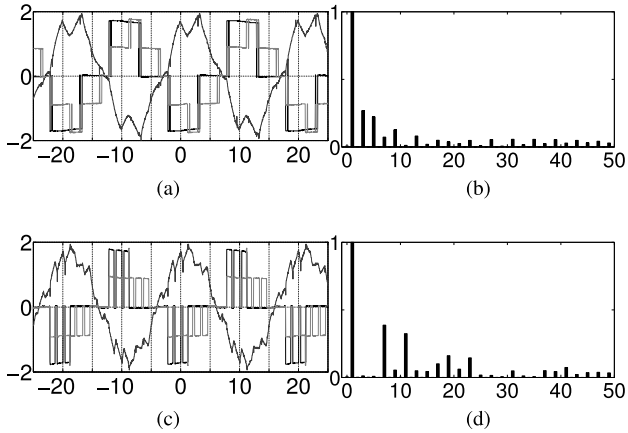

Fig. 7. Line current × 5, phase voltage × 100, line voltage × 200 (gray), and normalized frequency-domain representations corresponding to $m_a = 0.9$; time [ms]. Minimum phase-voltage THD CBM (a)–(b), SHE (c)–(d).

TABLE VI
EXPERIMENTAL INDICES SUMMARY

Index	CBM	SHE [47]	SOPWM [30]
Phase-Voltage THD	43.2%	59.6%	-
Line-Voltage THD	29.4%	58.1%	-
Phase-Voltage THD	102.9%	109.2%	116.4%
Line-Voltage THD	63.1%	85.0%	74.8%
Line-Current THD	13.1%	17.1%	20.8%

Minimum phase-voltage (gray background) and WTHD sequences corresponding to, respectively, $m_a = 0.9$ and $m_a = 0.5$.

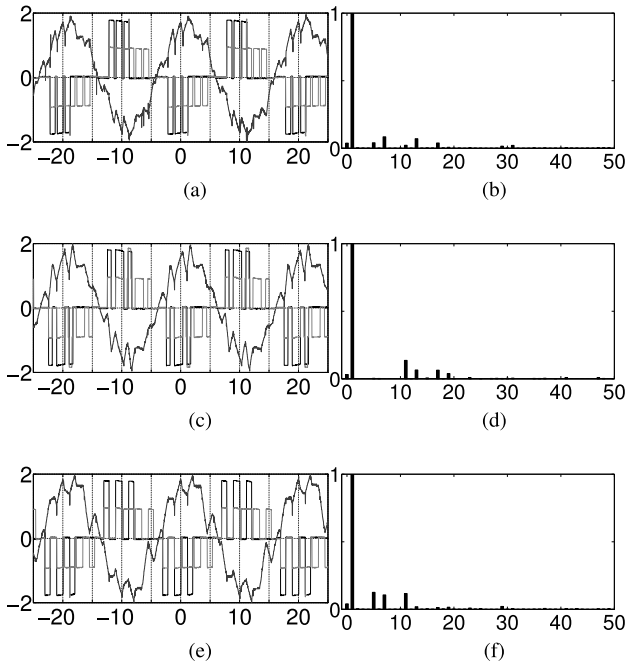

Fig. 8. Line current × 5, phase voltage × 100, line voltage × 200 (gray), and normalized frequency-domain representations corresponding to $m_a = 0.5$; time [ms]. Minimum WTHD CBM (a)–(b), SHE (c)–(d), SOPWM (c)–(d).

are summarized in Table VI. Line-currents THDs measured for the experimental waveforms are higher than the WTHD marks obtained in Section III-B. The difference between the two cases is attributed to the motor model and operation point. Nonetheless, both simulation and experimental results favor the CBM solution, with 22.8% improvement in WTHD and 23.1% improvement in line-current THD, over the SHE solution. As can be seen in the table, SOPWM obtained the highest line-current THD. These results emphasize the correlation between WTHD and line-current THD.

V. Conclusion

A performance-based modulation scheme was presented in this paper. The proposed CBM method utilizes a direct search over all valid switching sequences and locates the optimal sequence in reference to a given objective function. The CBM scheme ensures primacy of the selected solution over any other modulation technique commutating in an equal number of switching angles per fundamental cycle. CBM does not impose any limitation over modulation index. It could take into account practical inverter considerations, such as minimum turn ON and OFF times, and prevents the possibility of impractical solutions. Unlike other optimization-based PWM methods, CBM would always converge to the practical absolute extremum. The latter is true even when there exist switching angle discontinuities with respect to the modulation index. Simulation and experimental results presented in this paper validate the superiority of the CBM scheme over SHE and SOPWM methods.

While all waveforms presented in this paper maintain odd-function quarter wave symmetry, dropping waveform symmetry is feasible. By doing so, an extended solution set is obtained. Applying the CBM method to the new set may provide better inverter performances than those presented in this paper. Extending the CBM method to multilevel inverters follows similar lines. In both cases, the extended solution set would result in longer algorithm runtime.

Modulation index margin $\widetilde{m_a}$ is another advantage of the CBM algorithm. This liberty allows consideration of fundamental amplitudes within a given range. This, in turn, extends dramatically the feasible sequence candidates and may result in higher quality solutions.

Another notable advantage of the CBM solution is its ability to address multiple criteria marks. Incorporating two indices may be effective when both line-current THD and CMV are a quality factor. By minimizing both WTHD and phase-voltage THD, CBM could provide high quality line-current while keeping the CMV at bay.

Finally, although the CBM method was applied to VSIs, its application could be easily extended to CSIs.

Appendix A
Relation Between Phase-Voltage THD, Line-Voltage THD, and rms Values of the CMV

Following (7), the relation between phase-voltage THD, line-voltage THD, and rms values of the CMV could be expressed as follows:

$$\mathrm{THD}_{V_{\mathrm{Ph}}}^2 = \frac{\sum_{i=2}^{\infty} h_i^2}{h_1^2} = \frac{\sum_{\substack{i=2,\, i\neq 3k \\ k=1,2,\ldots}}^{\infty} \left(\sqrt{3}h_i\right)^2}{\left(\sqrt{3}h_1\right)^2} + \frac{\sum_{i=1}^{\infty} h_{3i}^2}{h_1^2}. \tag{10}$$

The rms value of the CMV is given by the zero-sequence (triplen) harmonics as follows:

$$\mathrm{CMV}_{\mathrm{RMS}} = \sqrt{\sum_{i=1}^{\infty} h_{3i}^2}. \tag{11}$$

The normalized index of the CMV would is defined as follows:

$$\mathrm{CMV}_{\mathrm{rms}} = \frac{\mathrm{CMV}_{\mathrm{RMS}}}{h_1}. \tag{12}$$

Therefore, the phase-voltage THD could be expressed by

$$\mathrm{THD}_{V_{\mathrm{Ph}}}^2 = \mathrm{THD}_{V_{\mathrm{Line}}}^2 + {\mathrm{CMV}_{\mathrm{rms}}}^2. \tag{13}$$

Appendix B
Example MATLAB Code for Solution Set Construction

Following is an example MATLAB code for the construction of the CBM solution set. An odd-function quarter wave symmetry with three angles per quarter fundamental cycle are assumed. amin and res are, respectively, minimum turn-on and turn-off and the desired angle resolution in radians. alph_res is closely related to the resolution capabilities of the controller

```
...
S = []; % empty solution set
for i = amin/2:res:pi/2-5/2*amin
    for j = i+amin:res:pi/2-3/2*amin
        for k = j+amin:res:pi/2-amin/2
            S = [S; i, j, k];
        end
    end
end
...
```

The complexity of the above code is $O\left(n^3\right)$. The solution set size $|\mathcal{S}|$ would equal $\frac{n\cdot(n+1)\cdot(n+2)}{3!}$, where

$$n = \left\lceil \frac{\pi}{2\cdot \mathrm{res}} \right\rceil. \tag{14}$$

Assuming three switching angles per quarter wave cycle and a desired angle resolution of 1°, n would be

$$n = \left\lceil \frac{\pi}{2\cdot \pi/180} \right\rceil = 90 \tag{15}$$

and the resulting solution set size would be

$$|\mathcal{S}| = \frac{90\cdot 91\cdot 92}{3!} = 125\,580. \tag{16}$$

Increasing the number of switching angles per quarter wave cycle would result in larger solution set size. The general case of N switching angles per quarter wave cycle involves $O\left(n^N\right)$

complexity and a solution set size of

$$|S| = \frac{(n+N-1)!}{(n-1)!N!}. \tag{17}$$

It should be kept in mind that the CBM algorithm is only performed once in an off-line mode. Hence, less attention was given to algorithm run-time in this paper. The optimization of the CBM search process and memory usage is to be explored in future research.

REFERENCES

[1] J. Rodriguez, J.-S. Lai, and F. Z. Peng, "Multilevel inverters: A survey of topologies, controls, and applications," *IEEE Trans. Ind. Electron.*, vol. 49, no. 4, pp. 724–738, Aug. 2002.

[2] J. Holtz, "Pulsewidth modulation-a survey," *IEEE Trans. Ind. Electron.*, vol. 39, no. 5, pp. 410–420, Oct. 1992.

[3] J. Rodriguez, S. Bernet, P. Steimer, and I. Lizama, "A survey on neutral-point-clamped inverters," *IEEE Trans. Ind. Electron.*, vol. 57, no. 7, pp. 2219–2230, Jul. 2010.

[4] J. Rodriguez, S. Bernet, B. Wu, J. Pontt, and S. Kouro, "Multilevel voltage-source-converter topologies for industrial medium-voltage drives," *IEEE Trans. Ind. Electron.*, vol. 54, no. 6, pp. 2930–2945, Dec. 2007.

[5] K. Corzine and J. Baker, "Multilevel voltage-source duty-cycle modulation: Analysis and implementation," *IEEE Trans. Ind. Electron.*, vol. 49, no. 5, pp. 1009–1016, Oct. 2002.

[6] N. Farokhnia, H. Vadizadeh, S. Fathi, and F. Anvariasl, "Calculating the formula of line-voltage THD in multilevel inverter with unequal dc sources," *IEEE Trans. Ind. Electron.*, vol. 58, no. 8, pp. 3359–3372, Aug. 2011.

[7] IEEE *Recommended Practices and Requirements for Harmonic Control in Electrical Power Systems*, *IEEE Std. 519-1992*, Apr. 1993.

[8] A. Hava and E. Ün andn,"A high-performance PWM algorithm for common-mode voltage reduction in three-phase voltage source inverters," *IEEE Trans. Power Electron.*, vol. 26, no. 7, pp. 1998–2008, Jul. 2011.

[9] Y.-S. Lai, P.-S. Chen, H.-K. Lee, and J. Chou, "Optimal common-mode voltage reduction PWM technique for inverter control with consideration of the dead-time effects—Part II: Applications to IM drives with diode front end," *IEEE Trans. Ind. Appl.*, vol. 40, no. 6, pp. 1613–1620, Nov./Dec. 2004.

[10] M. Dahidah, G. Konstantinou, N. Flourentzou, and V. Agelidis, "On comparing the symmetrical and non-symmetrical selective harmonic elimination pulse-width modulation technique for two-level three-phase voltage source converters," *IET Power Electron.*, vol. 3, no. 6, pp. 829–842, Nov. 2010.

[11] J. M. D. Murphy and M. Egan, "A comparison of PWM strategies for inverter-fed induction motors," *IEEE Trans. Ind. Appl.*, vol. IA-19, no. 3, pp. 363–369, May 1983.

[12] D. Holmes and T. Lipo, *Pulse Width Modulation for Power Converters: Principles and Practice*. Hoboken, NJ, USA: Wiley, 2003.

[13] D. Kostic, Z. Avramovic, and N. Ciric, "A new approach to theoretical analysis of harmonic content of PWM waveforms of single- and multiple-frequency modulators," *IEEE Trans. Power Electron.*, vol. 28, no. 10, pp. 4557–4567, Oct. 2013.

[14] L. Tolbert, F. Z. Peng, T. Cunnyngham, and J. Chiasson, "Charge balance control schemes for cascade multilevel converter in hybrid electric vehicles," *IEEE Trans. Ind. Electron.*, vol. 49, no. 5, pp. 1058–1064, Oct. 2002.

[15] K. Dagan and R. Rabinovici, "Sloped multi-level selective harmonic elimination pulse-width modulation," in *Proc. IEEE 26th Conv. Electr. Electron. Eng. Israel*, Nov. 2010, pp. 901–905.

[16] N. Yousefpoor, S. Fathi, N. Farokhnia, and H. Abyaneh, "THD minimization applied directly on the line-to-line voltage of multilevel inverters," *IEEE Trans. Ind. Electron.*, vol. 59, no. 1, pp. 373–380, Jan. 2012.

[17] O. Kukrer and H. Komurcugil, "Variable sampling frequency PWM waveforms," *IEEE Power Electron. Lett.*, vol. 1, no. 1, pp. 14–16, Mar. 2003.

[18] A. Julian, G. Oriti, and T. Lipo, "Elimination of common-mode voltage in three-phase sinusoidal power converters," *IEEE Trans. Power Electron.*, vol. 14, no. 5, pp. 982–989, Sep. 1999.

[19] P. C. Loh, D. Holmes, Y. Fukuta, and T. Lipo, "A reduced common mode hysteresis current regulation strategy for multilevel inverters," *IEEE Trans. Power Electron.*, vol. 19, no. 1, pp. 192–200, Jan. 2004.

[20] J. Kimball and M. Zawodniok, "Reducing common-mode voltage in three-phase sine-triangle PWM with interleaved carriers," *IEEE Trans. Power Electron.*, vol. 26, no. 8, pp. 2229–2236, Aug. 2011.

[21] D. Holmes, "The significance of zero space vector placement for carrier-based PWM schemes," *IEEE Trans. Ind. Appl.*, vol. 32, no. 5, pp. 1122–1129, Sep./Oct. 1996.

[22] M. Cacciato, A. Consoli, G. Scarcella, and A. Testa, "Reduction of common-mode currents in PWM inverter motor drives," *IEEE Trans. Ind. Appl.*, vol. 35, no. 2, pp. 469–476, Mar./Apr. 1999.

[23] J. Rodriguez, J. Pontt, P. Correa, P. Cortes, and C. Silva, "A new modulation method to reduce common-mode voltages in multilevel inverters," *IEEE Trans. Ind. Electron.*, vol. 51, no. 4, pp. 834–839, Aug. 2004.

[24] A. Hava and E. Un, "Performance analysis of reduced common-mode voltage PWM methods and comparison with standard PWM methods for three-phase voltage-source inverters," *IEEE Trans. Power Electron.*, vol. 24, no. 1, pp. 241–252, Jan. 2009.

[25] E. Un and A. Hava, "A near-state PWM method with reduced switching losses and reduced common-mode voltage for three-phase voltage source inverters," *IEEE Trans. Ind. Appl.*, vol. 45, no. 2, pp. 782–793, Mar./Apr. 2009.

[26] R. Tallam, R. Kerkman, D. Leggate, and R. Lukaszewski, "Common-mode voltage reduction PWM algorithm for ac drives," *IEEE Trans. Ind. Appl.*, vol. 46, no. 5, pp. 1959–1969, Sep./Oct. 2010.

[27] Y.-S. Lai and F.-S. Shyu, "Optimal common-mode voltage reduction PWM technique for inverter control with consideration of the dead-time effects—Part I: Basic development," *IEEE Trans. Ind. Appl.*, vol. 40, no. 6, pp. 1605–1612, Nov./Dec. 2004.

[28] N. Zhu, D. Xu, B. Wu, N. Zargari, M. Kazerani, and F. Liu, "Common-mode voltage reduction methods for current-source converters in medium-voltage drives," *IEEE Trans. Power Electron.*, vol. 28, no. 2, pp. 995–1006, Feb. 2013.

[29] Z. Zhao, Y. Zhong, H. Gao, L. Yuan, and T. Lu, "Hybrid selective harmonic elimination PWM for common-mode voltage reduction in three-level neutral-point-clamped inverters for variable speed induction drives," *IEEE Trans. Power Electron.*, vol. 27, no. 3, pp. 1152–1158, Feb. 2012.

[30] A. Rathore, J. Holtz, and T. Boller, "Synchronous optimal pulsewidth modulation for low-switching-frequency control of medium-voltage multilevel inverters," *IEEE Trans. Ind. Electron.*, vol. 57, no. 7, pp. 2374–2381, Jul. 2010.

[31] K. Dagan and R. Rabinovici, "Criteria-based modulation for power inverters," in *Proc. IEEE 27th Conv. Electr. Electron. Eng. Israel*, 2012, pp. 1–5.

[32] J. Holtz and X. Qi, "Optimal control of medium-voltage drives—An overview," *IEEE Trans. Ind. Electron.*, vol. 60, no. 12, pp. 5472–5481, Dec. 2013.

[33] Q. Jiang and T. Lipo, "Switching angles and dc link voltages optimization for multilevel cascade inverters," in *Proc. Int. Conf. Power Electron. Drives Energy Syst. Ind. Growth*, Dec. 1998, vol. 1, pp. 56–61.

[34] R. Ray, D. Chatterjee, and S. Goswami, "Harmonics elimination in a multilevel inverter using the particle swarm optimisation technique," *IET Power Electron.*, vol. 2, no. 6, pp. 646–652, Nov. 2009.

[35] C.-Y. Huang, T.-C. Chen, and C.-L. Huang, "A microcomputer-based induction motor drive system using current and torque control," *IEEE Trans. Energy Convers.*, vol. 14, no. 4, pp. 874–880, Dec. 1999.

[36] P. Tekwani, R. Kanchan, and K. Gopakumar, "Current-error space-vector-based hysteresis PWM controller for three-level voltage source inverter fed drives," *IEE Proc. - Electric Power Appl.*, vol. 152, no. 5, pp. 1283–1295, Sep. 2005.

[37] Y. Zhang, J. Long, Y. Zhang, T. Lu, Z. Zhao, and L. Jin, "Table-based direct power control for three-level neutral point-clamped pulse-width modulated rectifier," *IET Power Electron.*, vol. 6, no. 8, pp. 1555–1562, Sep. 2013.

[38] R.-S. Lai and K. Ngo, "A PWM method for reduction of switching loss in a full-bridge inverter," *IEEE Trans. Power Electron.*, vol. 10, no. 3, pp. 326–332, May 1995.

[39] X. Mao, R. Ayyanar, and H. Krishnamurthy, "Optimal variable switching frequency scheme for reducing switching loss in single-phase inverters based on time-domain ripple analysis," *IEEE Trans. Power Electron.*, vol. 24, no. 4, pp. 991–1001, Apr. 2009.

[40] Z. Du, L. Tolbert, and J. Chiasson, "Active harmonic elimination for multilevel converters," *IEEE Trans. Power Electron.*, vol. 21, no. 2, pp. 459–469, Mar. 2006.

[41] K. Dagan, R. Rabinovici, and D. Baimel, "An analytical approach to total harmonic distortion reduction in multi-level inverters," in *Proc. IEEE 26th Conv. Electr. Electron. Eng. Israel*, Nov. 2010, pp. 892–896.
[42] V. Agelidis, A. Balouktsis, I. Balouktsis, and C. Cossar, "Multiple sets of solutions for harmonic elimination pwm bipolar waveforms: Analysis and experimental verification," *IEEE Trans. Power Electron.*, vol. 21, no. 2, pp. 415–421, Mar. 2006.
[43] V. Agelidis, A. Balouktsis, and C. Cossar, "On attaining the multiple solutions of selective harmonic elimination PWM three-level waveforms through function minimization," *IEEE Trans. Ind. Electron.*, vol. 55, no. 3, pp. 996–1004, Mar. 2008.
[44] M. Di Piazza, A. Ragusa, and G. Vitale, "Power-loss evaluation in CM active EMI filters for bearing current suppression," *IEEE Trans. Ind. Electron.*, vol. 58, no. 11, pp. 5142–5153, Nov. 2011.
[45] C. Zhan, A. Arulampalam, and N. Jenkins, "Four-wire dynamic voltage restorer based on a three-dimensional voltage space vector pwm algorithm," *IEEE Trans. Power Electron.*, vol. 18, no. 4, pp. 1093–1102, Jul. 2003.
[46] P. Enjeti and R. Jakkli, "Optimal power control strategies for neutral point clamped (NPC) inverter topology," *IEEE Trans. Ind. Appl.*, vol. 28, no. 3, pp. 558–566, May/Jun. 1992.
[47] H. S. Patel and R. G. Hoft, "Generalized techniques of harmonic elimination and voltage control in thyristor inverters: Part I–harmonic elimination," *IEEE Trans. Ind. Appl.*, vol. IA-9, no. 3, pp. 310–317, May 1973.
[48] D. Shmilovitz, "On the definition of total harmonic distortion and its effect on measurement interpretation," *IEEE Trans. Power Del.*, vol. 20, no. 1, pp. 526–528, Jan. 2005.

Kfir J. Dagan received the B.Sc. degree in electrical and computer engineering, the B.Sc. degree in mathematics in 2006, the M.Sc. degree in electrical and computer engineering, and the Executive M.B.A degree in 2011, all from the Ben-Gurion University, Beer-Sheva, Israel, where he is currently working toward the Ph.D. degree in electrical and computer engineering.

From 1997 to 2000, he was a Project Director with the Signal Corps, Israeli Defense Forces. From 2004–2010, he was with the Israel Aircraft Industries (IAI), where he functioned as a System Engineer of the Magnetic Sensing Team and a Team Leader of the Control Systems Team. Since 2012, he has been an Adjunct Lecturer with the Electrical and Computer Engineering Department and the Energy Engineering Program, Ben-Gurion University. His current research interest includes power electronics, adjustable speed drives, electric machines, and harmonic phenomena in motor drive systems.

Mr. Dagan received the Joint Program for Mathematics & Electrical Engineering Scholarship for Outstanding Students (2003–2005), and the Society of Electrical and Electronics Engineers in Israel scholarship for outstanding Ph.D. students in 2012.

Raul Rabinovici was born in 1950. He received the Ph.D. degree from the Ben-Gurion University of The Negev, Beer Sheva, Israel, in 1987.

Since 1979, he has been with the Ben-Gurion University of The Negev, where he is an Associate Professor in the Department of Electrical and Computer Engineering. His research interests include power systems, electric machines, both as motors and generators, and industrial electronics. He has supervised more than 50 graduate students and published more than 170 papers in professional journals and conference proceedings.